Supporting Information for "Constraints on absolute chamber volume from geodetic measurements: Trapdoor faulting in the Galapagos"

Yujie Zheng[1], Laura Blackstone[2],Paul Segall[2]

[1]Division of Geological and Planetary Sciences, California Institute of Technology

[2]Geophysics Department, Stanford University

Contents of this file

1. Derivation
2. Figures S1 to S3
3. Conduit Model

References

Geist, D. J., Harpp, K. S., Naumann, T. R., Poland, M., Chadwick, W. W., Hall, M., & Rader, E. (2008). The 2005 eruption of Sierra Negra volcano, Galápagos, Ecuador. *Bulletin of Volcanology*, *70*(6), 655–673. doi: 10.1007/s00445-007-0160-3

Mastin, L. (1995). A numerical program for steady-state flow of Hawaiian magma-gas mixtures through vertical eruption conduits. *U. S. Geol. Surv. Open-File Report*, *pp*,

95–756.

Peterson, M. E., Saal, A. E., Kurz, M. D., Hauri, E. H., Blusztajn, J. S., Harpp, K. S., ... Geist, D. J. (2017). Submarine basaltic glasses from the Galapagos Archipelago: Determining the volatile budget of the mantle plume. *Journal of Petrology*, *58*(7), 1419–1450. doi: 10.1093/petrology/egx059

1. Derivations

Combining Eqn. [1b], [1c], [2b] and [2c], we can relate shear displacements $[\underline{\delta}_x; \underline{\delta}_y]$ to slips on the fault

$$\begin{bmatrix} \underline{\delta_x} \\ \underline{\delta_y} \end{bmatrix} = \begin{bmatrix} -J_{2x} & -J_{3x} \\ -J_{2y} & -J_{3y} \\ E & 0 \\ 0 & E \end{bmatrix}^{-1} \begin{bmatrix} J_{1x} \\ J_{1y} \\ N_x B \\ N_y B \end{bmatrix} \underline{s} \tag{1}$$

Combining Eqn. [1a] and [2a] and inverting yields the sill openings δ

$$\underline{\delta} = \begin{bmatrix} H \\ E \end{bmatrix}^{-1} \begin{bmatrix} -\Delta p \underline{1} - H_1 \underline{s} \\ N_z B \underline{s} \end{bmatrix} = \begin{bmatrix} Q_p & Q_f \end{bmatrix} \begin{bmatrix} -\Delta p \underline{1} - H_1 \underline{s} \\ N_z B \underline{s} \end{bmatrix} \tag{2}$$

where the latter form serves to define $[Q_p \;\; Q_f]$. The volume change of the sill can be computed by integrating the openings of the magma chamber:

$$\Delta V = \sum_i \delta_i dA_i = -\sum_i \left[dA_i \sum_j Q_{p_{ij}} \right] \Delta p + \sum_i \left[dA_i \sum_j [Q_f N_z B - Q_p H_1]_{ij} s_j \right] \tag{3}$$

where dA_i is the area of the i^{th} segment of the sill. Let

$$\Psi = -\sum_i \left[dA_i \sum_j Q_{p_{ij}} \right] \tag{4}$$

$$\Phi = \sum_i dA_i [Q_f N_z B - Q_p H_1]_{ij} \tag{5}$$

The surface measurements $\underline{u}$ resulting from the fault-chamber interaction can be described as

$$\underline{u} = G\underline{\delta} + G_1\underline{s} + G_2\underline{\delta_x} + G_3\underline{\delta_y} + \underline{\epsilon} \tag{6}$$

where G, G_1 G_2 and G_3 are Green's functions in the elastic half-space and $\underline{\epsilon}$ represents measurement errors. Replacing $\underline{\delta}$, $\underline{\delta_x}$ and $\underline{\delta_y}$ with Eqn. (2) and (1), we get

$$\begin{aligned}\underline{u} &= -GQ_p\underline{1}\Delta p + \left[G(Q_f N_z B - Q_p H_1) + G_1 + \begin{bmatrix} G_2 & G_3 \end{bmatrix} \begin{bmatrix} -J_{2x} & -J_{3x} \\ -J_{2y} & -J_{3y} \\ E & 0 \\ 0 & E \end{bmatrix}^{-1} \begin{bmatrix} J_{1x} \\ J_{1y} \\ N_x B \\ N_y B \end{bmatrix}\right]\underline{s} + \underline{\epsilon} \\ &= G_p\Delta p + G_s\underline{s} + \underline{\epsilon}\end{aligned} \tag{7}$$

The second equation serves to define the matrices G_p and G_s. Notice that the surface displacements are expressed in terms of a vector of fault slips along the trapdoor fault, and a scalar pressure change in the magma chamber.

2. Figures S1-S3

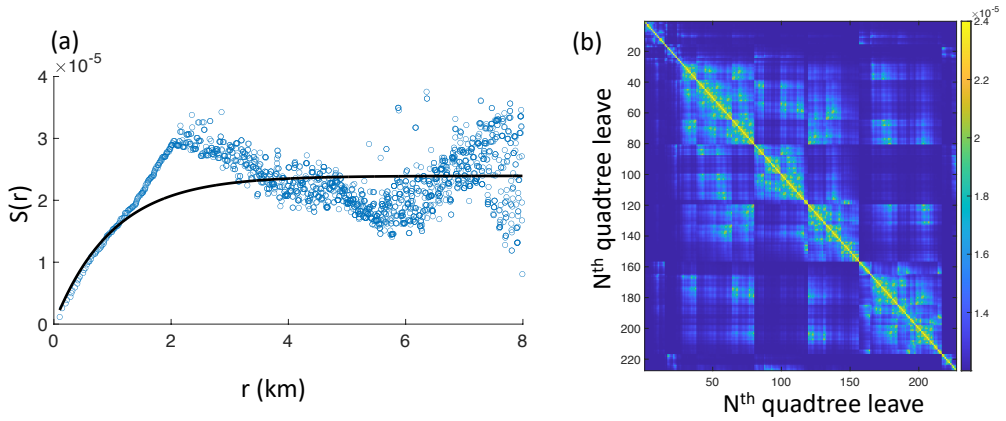

Figure S1. We use the non-deforming areas north of the caldera to estimate InSAR noise structure function and to derive an experimental covariance matrix. To reduce InSAR observations, we down-sample InSAR observations using a quadtree approach. (a) Structure function of InSAR noise. The black line is fit to the structure function. (b) Estimated covariance matrix for down-sampled InSAR quadtree leaves.

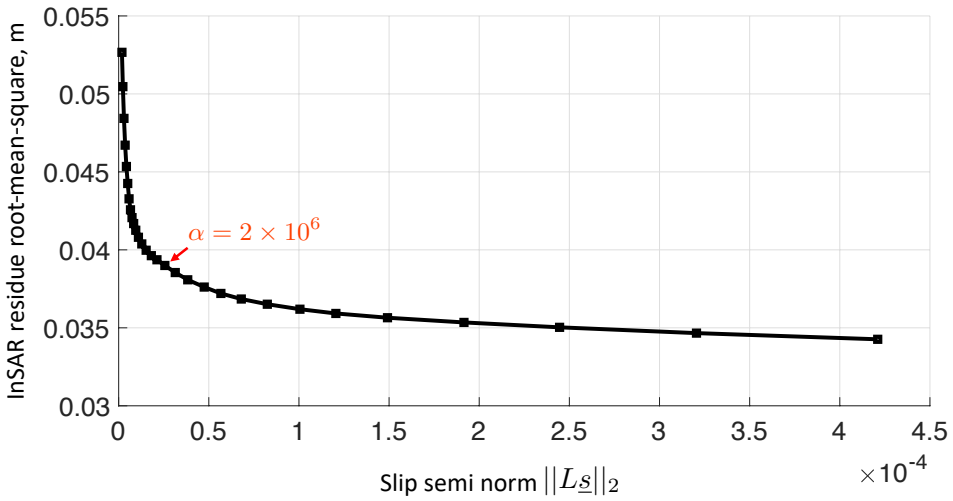

Figure S2. To determine the smoothness parameter, we fix the fault dip angle to be 88° northward and compute the L-curve with smoothness parameters varying from 10^5 to 10^8. The chosen smoothness parameter is marked by the red arrow.

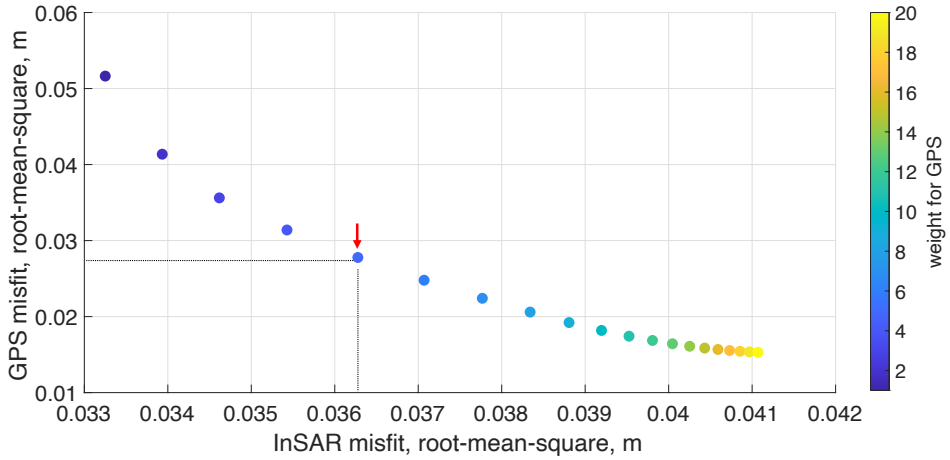

Figure S3. Data misfit as a function of weighting for GPS vs. InSAR data. We choose a weighting factor of 5 because it significantly reduces the misfit to the GPS data while not compromising goodness-of-fit for InSAR data too much.

3. Conduit Model

We assume a cylindrical conduit of constant radius r connecting the top of the magma reservoir to the surface. The governing equations are radially averaged to produce a one-dimensional, in depth, model. Flow below the fragmentation depth is laminar. The pressure at the base of the conduit is taken to be 54 MPa. Figure S4 shows a schematic of this model. The model does *not* allow for variations in conduit radius, relative motion of the bubble and liquid phases, the presence of a solid phase, or bubble-dependant viscosity.

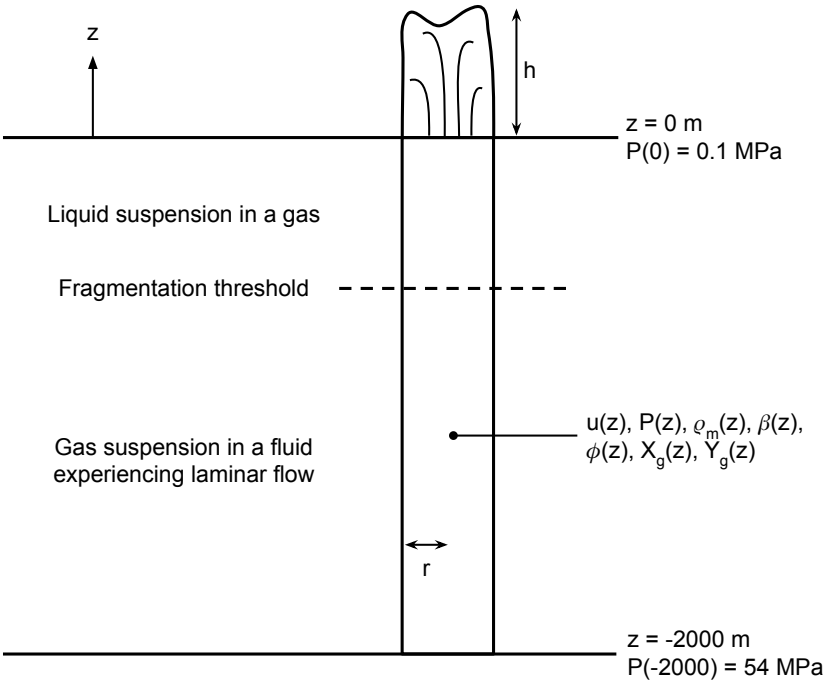

Figure S4. Schematic of conduit model showing radius r, fountain height h, mixture velocity u, pressure P, melt (liquid plus gas) density ρ_m, melt compressibility β_m, gas volume fraction ϕ, mass fraction of H_2O gas X_g, and mass fraction of CO_2 gas Y_g.

Magma in the conduit obeys conservation of mass and momentum. The former, $d(u\rho_m)/dz$, where u is the mixture velocity and ρ_m is density of the melt (liquid plus gas), can be recast as:

$$\frac{du}{dz} = -u\beta_m \frac{dP}{dz}[s^{-1}] \tag{8}$$

where P is pressure in Pa, z [m] is depth (positive in the up direction), β_m is the magma compressibility. Using this relationship, conservation of momentum can be written as

$$\frac{dP}{dz} = -\left(\rho_m g + 2\tau/r\right)\left(1 - u^2/c^2\right)^{-1}[Pa/m] \tag{9}$$

(Mastin, 1995), where $g = 9.81$ [m/s^2] is acceleration due to gravity, τ [N/m^2] is the wall shear stress, and $c = (\rho_m\beta_m)^{-1/2}$ [m/s] is the sound speed of the mixture.

The shear stress acting on the conduit wall is $\frac{1}{2}f_0\rho_m u^2$ [Pa] where f_0 is the Darcy-Weisbach friction factor, here assigned a value of 0.1. Shear stress due to laminar flow, below fragmentation, is $4\mu u/r$ [Pa], where μ is the magma viscosity. The total shear stress τ is thus:

$$\tau = \frac{1}{2}f_0\rho_m u^2 + 4\mu u/r[Pa] \textit{ below} \text{ fragmentation} \tag{10}$$

$$\tau = \frac{1}{2}f_0\rho_m u^2[Pa] \textit{ above} \text{ fragmentation} \tag{11}$$

Fragmentation occurs when the volume fraction of gas ϕ reaches 0.75.

To obtain equilibrium exsolution of H_2O and CO_2 we use the equilibrate function of MELTS applied to a typical Sierra Negra composition with varying volatile contents, at 1200°C, allowing only fluid and liquid phases. The composition used is sample D34a from (Peterson et al., 2017). The equilibrate function yields gas composition, liquid composition, melt density ρ_m, melt compressibility β_m, and gas volume fraction ϕ. To improve code efficiency, we create lookup tables relating the parameters of interest to $\log P$ for fixed total volatile content. Cubic spline interpo-

lation is used to determine quantities at intermediate pressures. The model assumes equilibrium exsolution continues to occur following fragmentation.

Volume flux refers to the volume of liquid exiting the top of the conduit per second, $\pi r^2 u_{z=0}(1-\phi_{z=0})$ [m^3/s]. The height of the lava fountain is calculated using the ballistic equation, $h = \frac{1}{2} g u_{z=0}^2$ [m].

3.1. Solution method

For a given volatile content and conduit radius, the code uses the shooting method to adjust the velocity at the bottom of the conduit until the pressure at the top of the conduit matches atmospheric pressure conditions. If no such solution can be found then a choked boundary condition, having a Mach number $M \equiv c^2/u^2$ of exactly 1 at the surface, is attempted. To integrate the equations in z, our Python implementation uses scipy.integrate.solve_ivp() with backwards differentiation, a relative tolerance of 1×10^{-12}, and an absolute tolerance of 1×10^{-12}. The conduit radius was adjusted for each volatile composition until the volume flux was within ± 3 m^3/s of 100 m^3/s to match the observed value in Geist et al. (2008).

3.2. Validation

Output from this code in the case of zero CO_2 is validated against the single volatile phase (water) model from Mastin (1995). Settings and parameters used in the benchmark model include the default Kilauea basalt composition, only liquid and gas phases, fixed radius with depth, lithostatic pressure in the chamber, atmospheric surface pressure, fragmentation at a gas volume fraction of 75%, equilibrium exsolution allowed after fragmentation, conduit length of 2000 m, and fixed temperature of 1200°C. Radius was adjusted for each volatile composition to

match a mass flux consistent with a 100 m^3/s volume flux. The output from the two models, shown in Figure S5, have reasonable agreement for all compositions considered.

Water (wt.%)	Benchmark fountain heights (m)	Calculated fountain height (m)	Deviation from benchmark
0.2	36	42	16.67%
0.3	78	68	-12.82%
0.4	107	95	-11.21%
0.5	139	123	-11.51%
0.6	173	151	-12.72%

Figure S5. Table comparing calculated fountain height for water-only compositions to output from Conflow (Mastin, 1995).